Article
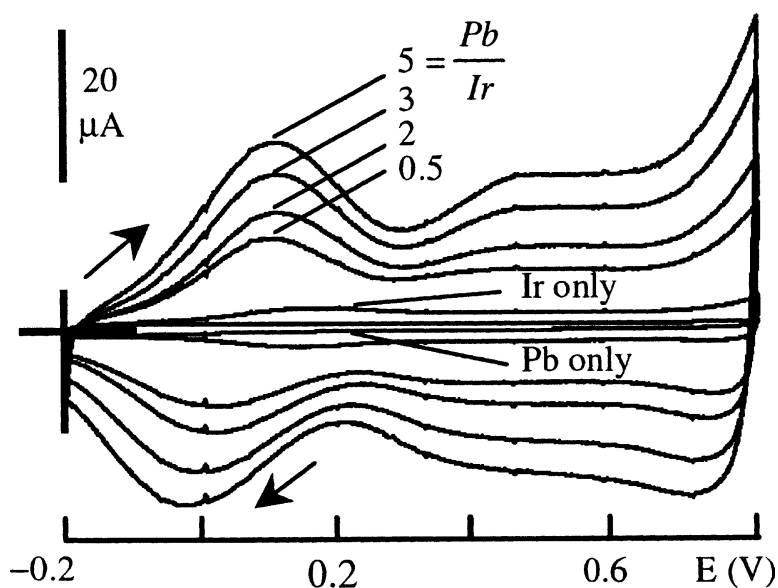
Synergistic Effects in Multicomponent Electrocatalysts: The Pb–Ir–O System

Conor Mullens, Michael Pikulski, Sabri Agachan, and Waldemar Gorski

More About This Article

Additional resources and features associated with this article are available within the HTML version:

- Supporting Information
- Access to high resolution figures
- Links to articles and content related to this article
- Copyright permission to reproduce figures and/or text from this article

View the Full Text HTML

Synergistic Effects in Multicomponent Electrocatalysts: The Pb−Ir−O System

Conor Mullens, Michael Pikulski, Sabri Agachan, and Waldemar Gorski*

Contribution from the Department of Chemistry, University of Texas at San Antonio, San Antonio, Texas 78249-0698

Received June 14, 2003; E-mail: wgorski@utsa.edu

Abstract: The ionic interactions were studied in aqueous solutions of Na_3IrCl_6 + $Pb(NO_3)_2$ in order to develop a facilitated electrosynthesis of iridium-based catalytic surfaces. Spectroscopic studies indicated that ion pair charge-transfer complexes $[IrCl_6^{3-}]-Pb(II)$ ($K = 6 \times 10^3$) and $[Ir(H_2O)Cl_5^{2-}]-Pb(II)$ ($K = 2 \times 10^3$) were formed in fresh and aged solutions, respectively. Electrochemical studies showed that interactions between the $Ir(H_2O)Cl_5^{2-}$ and Pb(II) species lead to synergistic lowering of the overpotential that was necessary for nucleation and growth of mixed metal oxide PbIrOx on the surface of glassy carbon electrodes. The Ir:Pb stoichiometry of the PbIrOx surface films was the same (1:1) as that of the high-temperature phase of Pb−Ir−O pyrochlore. Compared to IrOx, the PbIrOx films displayed enhanced catalytic activity toward the electrooxidation of carbohydrates. This was ascribed to synergism that involved retention of carbohydrate molecules at the Pb(II) sites of a PbIrOx film and oxidation at the adjacent Ir(IV) sites. The synergistic electroplating utilizing interactions between the partially aquated transition metal complex and posttransition metal ion represents a new synthetic route to highly homogeneous and reactive films of mixed metal oxides.

Introduction

Catalytic surfaces are essential in the development of electrochemical detectors, reactors, and fuel cells. Of particular interest are surfaces based on multicomponent electrocatalysts. In such materials, the properties of pure components may add up proportionally to their content if a phase mixture is obtained, or they may be amplified if an intimate homogeneous mixing or compound formation between the components is achieved. The latter condition, known as synergism, is an avenue of extraordinary potential for the development of new electrocatalysts with enhanced activity and/or stability.[1] Examples of inorganic materials that have been investigated for such purposes include metal alloys and metallic layers,[2−10] mixed or doped metal oxides,[11−21] metal−(metal oxides),[22−25] and cyanometalates−(metal oxides).[26−29]

The present paper describes synergistic effects that were discovered in the Pb−Ir−O redox system, both in aqueous solutions and in the solid state. The solid state of this system belongs to an important class of pyrochlore oxides, which display a remarkable variety of properties including electrocatalysis.[30−32] The powders of Pb−Ir−O pyrochlore oxides have been prepared by either the high-temperature solid-state synthesis[33,34] or precipitation from hot alkaline solutions.[35] The present study adds a new, mild electrosynthetic route to thin

(1) Trasatti, S. In *The Electrochemistry of Novel Materials*; Lipkowski, J., Ross, P. N., Eds; VCH Publishers: New York, 1994; Chapter 5.
(2) Yeo, I. H.; Johnson, D. C. *J. Electroanal. Chem.* **2001**, *495*, 110−119.
(3) Sun, Y.; Buck, H.; Mallouk, T. E. *Anal. Chem.* **2001**, *73*, 1599−1504.
(4) Wang, J.; Pamidi, P. V. A.; Cepria, G. *Anal. Chim. Acta* **1996**, *330*, 151−158.
(5) Krausa, M.; Vielstich, W. *J. Electroanal. Chem.* **1994**, *379*, 307−314.
(6) Marioli, J.; Kuwana, T. *Electroanalysis* **1993**, *5*, 11−17.
(7) Sun, S. G.; Lipkowski, J.; Altounian, Z. *J. Electrochem. Soc.* **1990**, *137*, 2443−2451.
(8) Goodenough, J. B.; Manoharan, R.; Shukla, A. K.; Ramesh, K. V. *Chem. Mater.* **1989**, *1*, 391−398.
(9) Sakamoto, M.; Takamura, K. *Bioelectrochem. Bioenerg.* **1982**, *9*, 571−582.
(10) Wittstock, G.; Strubing, A.; Szargan, R.; Werner, G. *J. Electroanal. Chem.* **1998**, *444*, 61−73.
(11) Popovic, N. D.; Cox, J. A.; Johnson, D. C. *J. Electroanal. Chem.* **1998**, *455*, 153−160.
(12) Feng, J.; Johnson, D. C. *J. Electrochem. Soc.* **1990**, *137*, 507−510.
(13) Yeo, I. H.; Johnson, D. C. *J. Electrochem. Soc.* **1987**, *134*, 1973−1977.
(14) Hsiao, Y. L.; Johnson, D. C. *J. Electrochem. Soc.* **1989**, *136*, 3704−3711.
(15) Velichenko, A. B.; Amadelli, R.; Baranova, E. A.; Girenko, D. V.; Danilov, F. I. *J. Electroanal. Chem.* **2002**, *527*, 56−64.
(16) Velichenko, A. B.; Girenko, D. V.; Kovalyov, S. V.; Gnatenko, A. N.; Amadelli, R.; Danilov, F. I. *J. Electroanal. Chem.* **1998**, *454*, 203−208.
(17) Bertoncello, R.; Cattarin, S.; Frateur, I.; Musiani, M. *J. Electroanal. Chem.* **2000**, *492*, 145−149.
(18) Cattarin, S.; Frateur, I.; Guerriero, P.; Musiani, M. *Electrochim. Acta* **2000**, *45*, 2279−2288.
(19) Gorski, W.; Kennedy, R. T. *J. Electroanal. Chem.* **1997**, *424*, 43−48.
(20) Rasiyah, P.; Tseung, A. C. C. *J. Electrochem. Soc.* **1983**, *130*, 365−368.
(21) Trasatti, S. In *Interfacial Electrochemistry: Theory, Experiment, and Applications*; Wieckowski, A., Ed.; Marcel Dekker: New York, 1999; Chapter 43 and references therein.
(22) de Tacconi, N. R.; Wenren, H.; McChesney, D.; Rajeshwar, K. *Langmuir* **1998**, *14*, 2933−2935.
(23) Savadogo, O.; Essalik, A. *J. Electrochem. Soc.* **1996**, *143*, 1814−1821.
(24) Shen, P. K.; Tseung, A. C. C. *J. Electrochem. Soc.* **1994**, *141*, 3082−3089.
(25) Kulesza, P. J.; Faulkner, L. R. *J. Electroanal. Chem.* **1989**, *259*, 81−98.
(26) Cataldi, T. R. I.; De Benedetto, G.; Bianchini, A. *J. Electroanal. Chem.* **1999**, *471*, 42−47.
(27) Du, G.; Lin, C.; Bocarsly, A. B. *Anal. Chem.* **1996**, *68*, 796−806.
(28) Cox, J. A.; Das, B. K. *J. Electroanal. Chem.* **1987**, *233*, 87−98.
(29) Cox, J. A.; Kulesza, P. J. *Anal. Chem.* **1984**, *56*, 1021−1027.
(30) Goodenough, J. B.; Manoharan, R.; Paranthaman, M. *J. Am. Chem. Soc.* **1990**, *112*, 2076−2082.
(31) Prakash, J.; Tryk, D. A.; Aldred, W.; Yeager, E. B. *J. Appl. Electrochem.* **1999**, *29*, 1463−1469.
(32) Zen, J.-M.; Kumar. A. S. *Acc. Chem. Res.* **2001**, *34*, 772−780.
(33) Longo, J. M.; Raccah, P. M.; Goodenough, J. B. *Mater. Res. Bull.* **1969**, *4*, 191−202.
(34) Kennedy, B. J. *J. Solid State Chem.* **1996**, *123*, 14−20.
(35) Horowitz, H. S.; Longo, J. M.; Horowitz, H. H.; Lewandowski, J. T. In *Solid State Chemistry in Catalysis*; Grasselli, R. K., Bradzdil, J. F., Eds.; American Chemical Society: Washington, DC, 1985.

films of such mixed oxides. Thin films are more compatible with the design of electrocatalytic surfaces and should display a better compositional and structural homogeneity than solid-state powders.

The electroplating of PbO_2 films modified with other species has been extensively investigated in the field of catalytic film electrodes. The PbO_2 has been used in such studies because of its good electrical conductivity, mechanical and chemical stability, ease of electrodeposition on various substrates, and high oxygen evolution overpotential. The PbO_2 has been doped with different ions (e.g., Bi(V), Fe(III), As(III), Co(II), Cl^-, F^-) in order to increase its electrocatalytic activity toward the oxidations involving O-transfer at high potentials.[11-16] Alternatively, the PbO_2 has been electroplated as a conductive matrix for immobilization of catalytic ruthenium and cobalt oxides for the O_2 evolution.[17,18]

The present work differs from the previous studies in that it focuses on the role of interactions between the posttransition metal (Pb) ion and transition metal (Ir) complex in the electroplating of intimately mixed metal oxide films (PbIrOx) on the surface of carbon electrodes. The lead–iridium interactions in a plating solution that led to facilitated electrodeposition of PbIrOx films were probed by spectroscopic and electrochemical methods. The PbIrOx surface films were characterized including their electrocatalytic activity toward the oxidation of mono- and disaccharides, which usually display slow redox kinetics at conventional surfaces. The enhancement of carbohydrate oxidation at PbIrOx films was discussed in terms of synergy between the lead and iridium sites of the film.

Experimental Section

Chemicals. The plating solutions were prepared using $Na_3IrCl_6 \cdot xH_2O$ (Ir 31.9%, Alfa Aesar), $Pb(NO_3)_2$ (Aldrich), and KNO_3 (Aldrich). The pH 7.40 phosphate buffer solutions (0.10 M) were made using NaH_2PO_4 (Fisher) and NaOH (Fisher). The carbohydrates D(−) arabinose, D(−) fructose, D(+) galactose, D(+) glucose, α-lactose, maltose, D(+) mannose, sucrose, and D(+) xylose were from Sigma. The water was purified with a Barnstead NANOpure cartridge system. The pyrochlore powder ($Pb_2Ir_2O_{7-x}$) was prepared by heating a mixture of IrO_2 (Aldrich) and PbO_2 (97+%, Aldrich) in a 1:1 molar ratio at 800 °C for 15 h in air. The X-ray diffraction pattern of the product displayed, in addition to small leftover peaks of iridium oxide, intense new peaks at 30.0° and 50.0° that confirmed the presence of the pyrochlore phase.

Instrumentation and Procedures. Electrochemical experiments were performed using the BAS (Bioanalytical Systems, Inc.) 100B/W Workstation and CH Instruments 832 Electrochemical Detector. The experiments were performed at room temperature (20 ± 1) in a conventional three-electrode system, with a Pt wire counter electrode, Ag/AgCl/3 M NaCl reference electrode (BAS), and a 3 mm diameter glassy carbon disk (BAS) as the working electrode.

Electronic spectra of solutions were recorded with the HP-8453 UV/visible diode array spectrophotometer. The Nonlinear Regression Analysis and Curve Fitting Program (NLREG) was used for fitting a theoretical equation to UV/visible spectroscopic data in order to calculate formation constants for the lead–iridium complexes.

The energy-dispersive X-ray (EDX) microanalysis was performed using an Oxford Instruments INCA unit. The X-ray diffraction (XRD) analysis was conducted on a Scintag XDS 2000 diffractometer equipped with a Peltier detector. Micrographs of the films were collected with a JEOL 840A Scanning Electron Microscope.

A flow injection system consisted of a reservoir of carrier solution connected to a six-port valve (Upchurch) equipped with a sample loop of ~200 μL. The outlet of the valve was connected to an electrochemi-
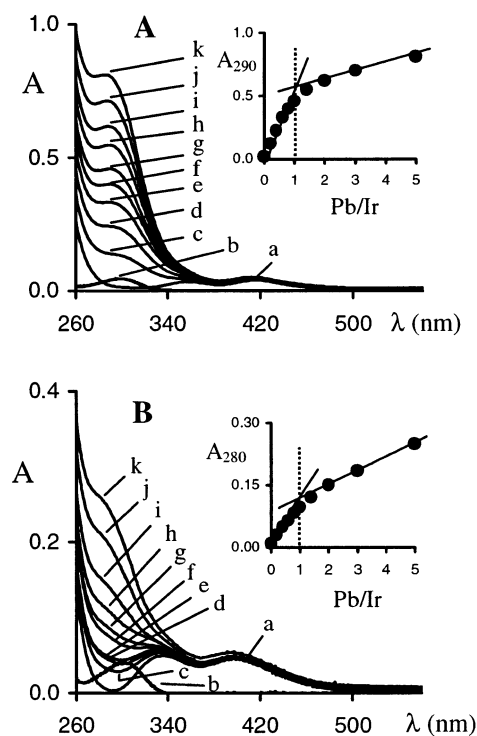
Figure 1. UV/visible spectra of fresh (A) and aged (B) solution of (a) 0.50 mM Na_3IrCl_6 and (b) 2.5 mM $Pb(NO_3)_2$. Solutions of salt mixtures contained 0.50 mM Na_3IrCl_6 and (c) 0.1, (d) 0.2, (e) 0.3, (f) 0.4, (g) 0.5, (h) 0.7, (i) 1.0, (j) 1.5, and (k) 2.5 mM $Pb(NO_3)_2$. Insets: Plots of absorbance vs molar ratio of lead to iridium salt in a solution.

cal cell using Teflon tubing. The working electrode was positioned at the outlet of the tubing. The carrier solution was gravity fed at 2.0 mL min^{-1}. All experiments were repeated at least 3 times, and the means of measurements are presented with the standard deviations.

Electroplating of Surface Films. All of the films were prepared at room temperature by applying 1.200 V for 15 min to glassy carbon electrodes immersed in quiescent plating solutions (pH 6.0). The PbOx, IrOx, and PbIrOx films were formed using the plating solutions that contained the $Pb(NO_3)_2$, Na_3IrCl_6, and $Pb(NO_3)_2$ + Na_3IrCl_6 salts, respectively. The 0.10 M KNO_3 was used as a background electrolyte. Both freshly prepared and aged plating solutions were used. The aged solutions were prepared by heating at 80 °C for 1 h in tightly closed glass vials. The heat-induced aquation equilibrium was preserved by cooling solutions to room temperature before further experimentation.

Prior to experiments, the glassy carbon electrodes were wet polished on 3M sand paper (Grain 2000) and a polishing cloth (Mark V Lab) with alumina particles (0.3 and 0.05 μm diameter) suspended in water. The slurry that accumulated on the electrode surface was removed by a 30 s ultrasonication in water.

Results and Discussion

UV/visible Spectroscopy of the Pb(II)–Ir(III) System in Aqueous Solutions. The electronic spectrum of a fresh Na_3IrCl_6 solution (Figure 1A, curve a) displayed two absorption bands at 355 and 414 nm due to the spin allowed $^1A_{1g} \rightarrow {}^1T_{2g}$ and $^1A_{1g} \rightarrow {}^1T_{1g}$ d–d transitions within the iridium center.[36] In the aged solution, these absorption bands were shifted toward shorter wavelengths (Figure 1B, curve a). Such a hypsochromic shift in absorption bands indicated a substitution of a chloride with a stronger H_2O ligand in the first coordination sphere of the $IrCl_6^{3-}$ complex. Considering recent studies[37] on the speciation of iridium chlorocomplexes and the electrochemical

(36) Jorgensen, C. K. *Acta Chem. Scand.* **1956**, *10*, 500–508.

data discussed below, this aquation process can be represented as $IrCl_6^{3-} \rightleftharpoons Ir(H_2O)Cl_5^{2-} + Cl^-$.

The electronic spectra of iridium complexes changed in the presence of lead ions, even though the Pb(II) ions alone displayed only a minor absorbance in both fresh and aged solutions (Figure 1, curves b). The general notation Pb(II) will be used throughout this discussion to describe the lead(2+) aquaion, which probably could undergo a partial hydrolysis. The absorbance of both iridium complexes, the $IrCl_6^{3-}$ in fresh solutions (Figure 1A, curves c−k) and $Ir(H_2O)Cl_5^{2-}$ in aged solutions (Figure 1B, curves c−k), increased with addition of Pb(II) ions. Such spectral changes indicated the presence of interactions between the Pb(II) ions and iridium complexes.

Figure 1 shows two significant aspects of the influence that Pb(II) ions exerted on the absorbance of iridium complexes. First, the Pb(II) ions amplified only the short-wavelength absorbance at <370 nm. The absorbance at >370 nm, which was due to d−d transitions within the iridium center, remained unchanged. The latter suggested that the first coordination sphere of iridium complexes remained intact in the presence of Pb(II) ions and, thus, argued for the outer-sphere interactions between the iridium complexes and Pb(II) ions. Therefore, the increase in absorbance at <370 nm can be ascribed to Pb(II)-enhanced ligand-to-iridium charge-transfer (CT) transitions in the $[IrCl_6^{3-}]$−Pb(II) and $[Ir(H_2O)Cl_5^{2-}]$−Pb(II) bridged species that were formed in fresh and aged solutions, respectively. Similar enhancement in absorbance has been observed previously in the case of halogen-bridged mixed-valence complexes of transition metals, for example, Pd(II)-enhanced Cl-to-Pt CT transitions in the single crystals of $[(en)_2Pt(\mu-Cl)_2Pd(en)_2](ClO_4)_4$.[38]

The second notable aspect of Pb(II)-induced changes in the spectra of iridium complexes was a much larger increase (~3 times) in absorption intensity of the fresh (Figure 1A) than aged (Figure 1B) solutions. We hypothesized that this was caused by a different bridging of Pb(II) ions to Ir(III) complexes, e.g. $Ir(\mu-Cl)_2Pb$ and $Ir(\mu-Cl)(\mu-O)Pb$ cores in fresh and aged solutions, respectively. In such a scenario, the difference in absorbance intensity of the two solutions could be explained by a stronger enhancement of the Cl-to-Ir than O-to-Ir CT transitions by the Pb(II) ion bridged to Cl and O atom, respectively. The nuclear magnetic resonance and mass spectrometric studies of bridging between the Ir and Pb centers will be reported separately.

The stoichiometry of interactions between the Pb(II) ions and iridium complexes was analyzed using the mole-ratio method. The analysis involved spectra of 10 solutions, each of which contained a constant concentration of the iridium complex (0.50 mM) and a different concentration of Pb(II) ions ranging from 0 to 2.50 mM. The overlaid spectra displayed a pseudo-isosbestic point at ~370 nm (Figure 1), which suggested the presence of two dominant absorbing species, the iridium and iridium−lead charge-transfer complexes. Insets in Figure 1 show the plots of absorbance *A* versus Pb/Ir molar ratio using the absorbance at 290 and 280 nm for fresh and aged solutions, respectively. The extrapolated linear portions of such plots crossed at Pb/Ir = 1.0 ± 0.1, which indicated a stoichiometry

(37) Sanchez, J. M.; Salvado, V.; Havel, J. *J. Chromatogr. A* **1999**, *834*, 329−340.
(38) Wada, Y.; Mitani, T.; Toriumi, K.; Yamashita, M. *J. Phys. Soc. Jpn.* **1989**, *58*, 3013−3121.
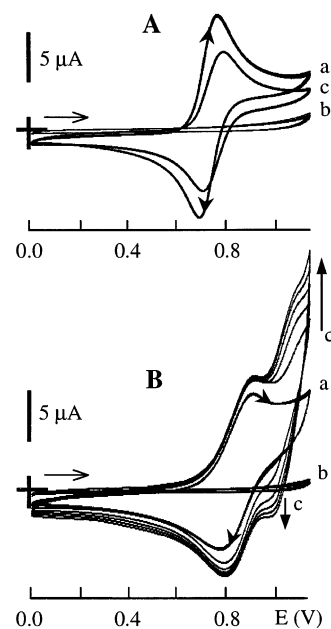
Figure 2. Cyclic voltammograms (first 5 cycles) recorded at a bare glassy carbon electrode in fresh (A) and aged (B) solutions of (a) 1.0 mM Na₃-IrCl₆, (b) 0.50 mM Pb(NO₃)₂, and (c) 1.0 mM Na₃IrCl₆ + 0.50 mM Pb-(NO₃)₂. Background electrolyte, 0.10 M KNO₃. Scan rate, 50 mV s⁻¹.

of 1:1 for the iridium−lead complexes. That the slope beyond the Pb/Ir = 1 point was greater than zero indicated formation of an increasing amount of iridium−lead complex in the presence of excess Pb(II) ions in a solution.

The formation constants *K* for the $[IrCl_6^{3-}]$−Pb(II) and $[Ir(H_2O)Cl_5^{2-}]$−Pb(II) charge-transfer complexes were determined by fitting the following equation, which was derived for the 1:1 stoichiometry, to the experimental spectroscopic data shown in Figure 1

$$C_{Pb} = (A - A_0)\left[\frac{1}{K(A_{max} - A)} + \frac{C_{Ir}}{(A_{max} - A_0)}\right] \quad (1)$$

where C_{Pb} and C_{Ir} are analytical concentrations of the Pb(II) ion and iridium complex in a solution, A_0 and A are absorbances (at 290 or 280 nm) of the iridium complex in the absence and presence of Pb(II) ions, respectively, and A_{max} is the absorbance of the iridium complex in the presence of a 10× excess of Pb-(II) ions. The curve fitting was performed on a series of seven different Pb/Ir molar ratios ranging from 0.2 to 2.0 ($R^2 \geq 0.997$, RSD < 4%). This procedure yielded formation constants equal to 6×10^3 and 2×10^3 for the $[IrCl_6^{3-}]$−Pb(II) and $[Ir(H_2O)Cl_5^{2-}]$−Pb(II) complex, respectively. Such formation constants indicated moderately strong interactions between the Pb(II) ions and iridium complexes. For example, using $K = 2 \times 10^3$ one can calculate that ~40% of iridium complex was bridged to Pb(II) ions in the aged solution with the ratio Pb/Ir = 1.

Voltammetry of the Pb(II)−Ir(III) System in Aqueous Solutions. Figure 2 presents cyclic voltammograms recorded at a bare glassy carbon electrode in the fresh (A) and aged (B) solutions of Na₃IrCl₆ (curve a), Pb(NO₃)₂ (curve b), and Na₃-IrCl₆ + Pb(NO₃)₂ (curve c) salts. Each voltammogram was composed of five consecutive potential−current (*E*−*I*) cycles that were recorded in a given solution. The upper potential limit was set at 1.100 V in order to avoid the electrodeposition of IrOx and PbOx on the electrode surface at high positive

potentials from solutions of Na_3IrCl_6 and $Pb(NO_3)_2$ salts, respectively. The symbols IrOx and PbOx refer here to hydrated oxides IrO_2 and PbO_2, which can be represented in various ways.[39,40]

Cyclic voltammetry in a fresh solution of Na_3IrCl_6 (Figure 2A, curve a) yielded a reversible pair of current peaks ($\Delta E = 60 \pm 2$ mV) for the $IrCl_6^{2-}/IrCl_6^{3-}$ couple at a mid-peak potential of 0.700 V. In the aged solution (Figure 2B, curve a), the voltammogram displayed a pair of current peaks at 0.820 V. Based on our previous work,[41] the 0.120 V shift in the mid-peak potential corresponded to the aquation of one chloride ligand in the first coordination sphere of the $IrCl_6^{3-}$ complex. Thus, the current peaks at 0.820 V can be ascribed to the $Ir(H_2O)Cl_5^{-}/Ir(H_2O)Cl_5^{2-}$ redox couple.

The Pb(II) ions were electrochemically silent in the selected potential window (Figure 2, curves b). This indicated that the oxidation of Pb(II) to PbO_2 required a large overpotential since the reversible potential of the PbO_2/Pb(II) couple was 0.64 V under the experimental conditions used (pH 6.0, $C_{Pb(II)} = 0.50$ mM). Nevertheless, the presence of Pb(II) ions in the solution changed the voltammograms of iridium complexes. In a fresh solution, the current peaks due to the redox of the iridium couple shifted slightly ($\sim$0.02 V) toward more positive potentials and decreased by $\sim$30% in the presence of Pb(II) ions (Figure 2A, curve c). Because the peaks' separation did not change and no precipitation was observed in the solution, the decrease in current peaks was ascribed to a lower diffusion coefficient of the $[IrCl_6^{3-}]-Pb(II)$ complex.

In the aged solution, the effect of Pb(II) ions on the voltammogram of iridium complex was more dramatic as illustrated by an extra current that was observed at potentials more positive than 0.90 V (Figure 2B, curve c). In addition, this extra current increased on consecutive potential scans. Such an increase in current was indicative of an electroactive deposit being formed on the surface of the glassy carbon electrode already at relatively low potentials ($>$0.90 V). Apparently, the bridging of the Pb(II) ion to $Ir(H_2O)Cl_5^{2-}$ complex in the aged solution diminished the overpotential necessary for the nucleation and growth of a mixed metal oxide on the electrode surface.

The nucleation of surface deposit from the aged solution, and not from the fresh one, underscored the difference in reactivity of iridium−lead complexes in the two solutions. This observation, along with UV/visible data, supported a notion that charge-transfer processes in the iridium−lead complexes were tuned by different bridging atoms, that is, Ir−Cl−Pb and Ir−O−Pb cores in fresh and aged solutions, respectively. Thus, the decrease in nucleation overpotential in the aged solution was hypothesized to arise from structural similarities between the reactant in a solution (Ir−O−Pb core) and the product on the electrode surface (PbIrOx film). Consequently, the electroplating of mixed metal oxide PbIrOx was triggered by relatively low potentials applied to the electrode ($>$0.90 V). Such a facilitated electroplating can be considered synergistic because the electroplating of single metal oxides IrOx and PbOx required much larger overpotentials ($>$1.15 V) under the same experimental conditions.
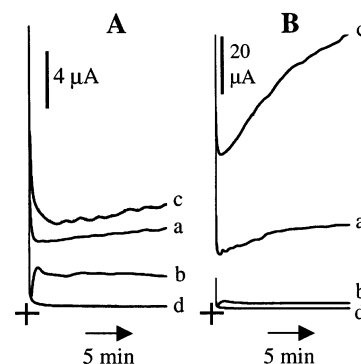
Figure 3. Current vs time curves ($E = 1.200$ V) recorded at a bare glassy carbon electrode in fresh (A) and aged (B) solutions of (a) 1.0 mM Na_3IrCl_6, (b) 0.50 mM $Pb(NO_3)_2$, and (c) 1.0 mM Na_3IrCl_6 + 0.50 mM $Pb(NO_3)_2$. Curves d were obtained in a 0.10 M KNO_3 background electrolyte solution.

Electroplating of Metal Oxide Films from Solutions of Ir(III) and Pb(II) Ions. The metal oxide films were electroplated on the surface of glassy carbon electrodes using a constant potential of 1.200 V. At such a potential, both single oxides IrOx and PbOx and a mixed oxide PbIrOx were deposited on the surface of glassy carbon electrodes (vide infra). The comparative analysis of currents recorded during the deposition of IrOx, PbOx, and PbIrOx films was used to discern the synergistic effects involved in the formation of PbIrOx films.

Figure 3 shows two sets of current−time (I−t) curves that were recorded at a glassy carbon electrode immersed in either fresh (Figure 3A) or aged (Figure 3B) plating solutions. Each set consisted of I−t curves recorded in solutions of Na_3IrCl_6 (curve a), $Pb(NO_3)_2$ (curve b), and Na_3IrCl_6 + $Pb(NO_3)_2$ (curve c) salts. The EDX analysis revealed that in the course of recording curves a, b, and c the glassy carbon electrodes were covered with deposits containing the iridium, lead, and iridium + lead species, respectively.

The comparison of curves a in Figure 3A and B revealed that the aging of Na_3IrCl_6 solution increased the electroplating current. Such an effect has been previously observed and ascribed to more efficient formation of the IrOx surface film from a solution of partially aquated $Ir(H_2O)Cl_5^{2-}$ complex than from a solution of the original $IrCl_6^{3-}$ complex.[41] In contrast, the aging of the $Pb(NO_3)_2$ solution had no detectable effect on the I−t transients (curves b). The transients displayed a classical shape, which corresponded to the case of progressive nucleation and three-dimensional growth of PbOx films with an induction time.[42]

In fresh solutions (Figure 3A), the electroplating currents were additive, that is, the current recorded in a solution of Na_3IrCl_6 + $Pb(NO_3)_2$ salt mixture (curve c) was approximately equal to the sum of currents obtained in solutions of individual salts Na_3IrCl_6 (curve a) and $Pb(NO_3)_2$ (curve b). Indeed, the integration of curves a, b, and c yielded electroplating charges Q_{IrOx}, Q_{PbOx}, and Q_{PbIrOx}, respectively, which gave the ratio $Q_{PbIrOx}/(Q_{IrOx} + Q_{PbOx})$ equal to 0.9 ± 0.1 ($N = 4$). This indicated an independent electroplating of PbOx and IrOx from an aqueous mixture of Na_3IrCl_6 + $Pb(NO_3)_2$ salts. Evidently, the interactions between the $IrCl_6^{3-}$ and Pb(II) ions in a solution (Ir−Cl−Pb) were of no consequence for the electroplating process from freshly prepared solutions.

(39) Burke, L. D.; Mulcahy, J. K.; Whelan, D. P. *J. Electroanal. Chem.* **1984**, *163*, 117−128.
(40) Ruetschi, P. *J. Electrochem. Soc.* **1992**, *139*, 1347−1355.
(41) Pikulski, M.; Gorski, W. *Anal. Chem.* **2000**, *72*, 2696−2702.
(42) Gonzalez-Garcia, J.; Gallud, F.; Iniesta, J.; Montiel, V.; Aldaz, A.; Lasia, A. *Electroanalysis* **2001**, *13*, 1258−1264.
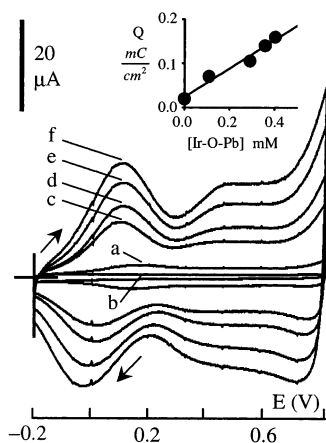
Figure 4. Cyclic voltammograms recorded in pH 7.40 phosphate buffer at glassy carbon electrodes (50 mV s^{-1}). Prior to recordings, the electrodes were held at 1.200 V for 15 min in aged plating solutions of individual salts (a) 0.50 mM Na_3IrCl_6 and (b) 0.50 mM $Pb(NO_3)_2$ and in solutions of salt mixtures that contained 0.50 mM Na_3IrCl_6 and (c) 0.25, (d) 1.0, (e) 1.6, and (f) 2.5 mM $Pb(NO_3)_2$. Inset: Plot of charge Q obtained from integration of curves a and c–f vs concentration of $[Ir(H_2O)Cl_5{}^{2-}]$–Pb(II) complex in solutions a and c–f calculated using $K = 2 \times 10^3$.

In the aged solutions (Figure 3B), the electroplating currents did not add up. The ratio of electroplating charges $Q_{PbIrOx}/(Q_{IrOx} + Q_{PbOx})$ was equal to 3.0 ± 0.3 ($N = 4$). The ratio larger than one indicated a synergistic amplification of a constant potential electroplating of the PbIrOx film (curve c). The amplification can be rationalized in terms of a three-channel electroplating at 1.200 V, which involved the oxidation of the $[Ir(H_2O)Cl_5{}^{2-}]$–Pb(II) charge-transfer complex, $Ir(H_2O)Cl_5{}^{2-}$ complex, and Pb(II) ion. Considering a lower overpotential for the oxidative electroplating of the charge-transfer complex (Figure 2B, curve c), the condition $Q_{PbIrOx} > Q_{IrOx} + Q_{PbOx}$ was due to faster oxidation of the $[Ir(H_2O)Cl_5{}^{2-}]$–Pb(II) than $Ir(H_2O)Cl_5{}^{2-}$ and Pb(II) species at the electrode surface. The following three studies supported the hypothesis of Pb(II)-promoted electroplating of PbIrOx on the electrode surface from aged solutions.

Voltammetric Characterization of PbIrOx Films. The PbIrOx films were prepared using aged plating solutions that contained a constant concentration of iridium complex and a different concentration of Pb(II) ions. Figure 4 shows fingerprint voltammograms of such films (curves c–f). The current peaks and shape of voltammograms were typical for activated iridium electrodes,[39,43] which indicated that iridium(IV) oxide was a redox active component in the PbIrOx films. Indeed, the Pb(II) ions were electrochemically silent in the selected potential window and alone did not form a stable surface film (curve b). However, they dramatically increased the amount of PbIrOx deposit on the electrode surface (curves c–f) when compared to the amount of IrOx that was electroplated from the Pb(II)-free plating solution (curve a).

The amount of PbIrOx on the electrode surface was quantified in terms of charge Q, which was obtained by integrating voltammograms c–f from −0.20 to 0.60 V. The inset in Figure 4 shows that the charge Q was directly proportional to the concentration of the $[Ir(H_2O)Cl_5{}^{2-}]$–Pb(II) complex in a corresponding plating solution calculated using $K = 2 \times 10^3$. Such a relationship suggested that electroplating of PbIrOx films

(43) Conway, B. E.; Mozota, J. *Electrochim. Acta* **1983**, *28*, 9–16.
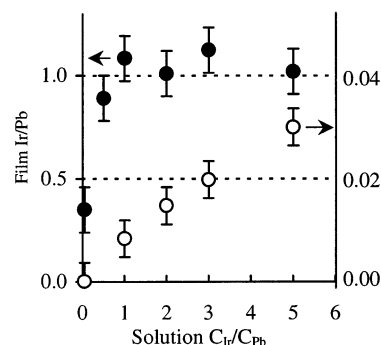
Figure 5. Dependence of Ir/Pb atomic ratio in PbIrOx films, as revealed by EDX analysis, on the molar ratio of iridium and lead salts C_{Ir}/C_{Pb} in fresh (○) and aged (●) plating solutions ($C_{Pb=const} = 0.5$ mM).

indeed proceeded via a fast oxidation of the iridium–lead complex.

EDX and SEM Analysis of PbIrOx Films. Consistent with the above, the atomic ratio Ir/Pb in the films, plated from aged solutions (Figure 5, closed circles), was constant and close to a 1:1 stoichiometry of the $[Ir(H_2O)Cl_5{}^{2-}]$–Pb(II) complex. Only a solution with a ratio $C_{Ir}/C_{Pb} = 0.05$ yielded a film with a smaller Ir/Pb ratio (= 0.4), which could be explained by a codeposition of PbOx due to a large excess of free Pb(II) ions in such a solution.

The films prepared from fresh solutions displayed an atomic ratio Ir/Pb much lower than the solution ratio C_{Ir}/C_{Pb} (Figure 5, open circles), which was indicative of a very inefficient electroplating of iridium oxide. However, both ratios were proportional to each other, which indicated that films were formed by an independent oxidation of the Pb(II) and $IrCl_6{}^{3-}$ ions at the electrode surface. Evidently, a slow oxidation of the $[IrCl_6{}^{3-}]$–Pb(II) complex did not affect the Ir/Pb ratio in such films.

The SEM micrographs showed a distinct morphological difference between deposits that were electroplated from fresh and aged solutions. The fresh solutions yielded granular films with a grain diameter equal to ~0.2 μm. The films formed from aged solutions were practically featureless at the same magnification, which suggested high surface uniformity.

The XRD experiments were performed in order to investigate the structure of PbIrOx films that were electroplated from aged solutions. However, the XRD patterns displayed only broad bands of low intensity, which indicated a microcrystalline/amorphous nature and small thickness of the films and, thus, precluded their structural analysis.

Cathodic Stripping of PbIrOx Films. Figure 6 shows the cathodic stripping voltammograms of a reference PbOx film and two films PbIr$_y$Ox and PbIrOx that were prepared using either a fresh (film I) or aged (film II) plating solution. Stripping of the reference PbOx film into a background electrolyte solution resulted in a narrow symmetrical peak at 0.52 V (curve a), which was due to dissolution of the PbOx according to Pb(IV)$_{film}$ + 2e$^-$ → Pb(II)$_{solution}$.

Stripping of film I yielded a peak at the same potential of 0.52 V (curve b), which indicated dissolution of a PbOx phase from the PbIr$_y$Ox film. That the peak on curve b was wider than the reference peak suggested some interaction between the PbOx and IrOx phases in the film. In contrast to this phase mixture scenario, no separate PbOx phase existed in film II as indicated by the lack of Pb(IV) → Pb(II) stripping peak (curve
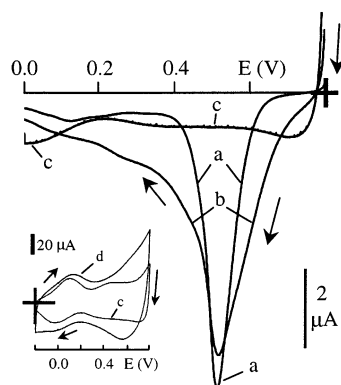
Figure 6. Cathodic stripping voltammograms (2 mV s^{-1}) of a reference PbOx film electroplated from 0.50 mM Pb(NO$_3$)$_2$ solution (a) and of two PbIrOx films electroplated from fresh (b) and aged (c) plating solutions that contained 0.50 mM Pb(NO$_3$)$_2$ + 1.0 mM Na$_3$IrCl$_6$. Inset: Cyclic voltammograms (50 mV s^{-1}) recorded at the (c) PbIrOx film electrode after the stripping experiment c and (d) high-temperature Pb−Ir−O pyrochlore film prepared using chitosan as an immobilization matrix. Background electrolyte, pH 7.40 phosphate buffer.

Figure 7. Flow injection analysis ($E = 0.750$ V) of 3.0 mM carbohydrate solutions at PbIrOx (I), and IrOx (II) film electrodes: (a) maltose, (b) glucose, (c) mannose, (d) xylose, (e) fructose, (f) galactose, (g) lactose, (h) arabinose, (i) sucrose, and (j) blank injections. Carrier solution, pH 7.40 phosphate buffer.

c). Apparently, the lead in the film existed mostly as Pb(II) sites, which were electrochemically silent in the selected potential window. The current seen on curve c was due to the reduction process Ir(IV) → Ir(III). The latter did not result in dissolution of the PbIrOx phase as indicated by a stable cyclic voltammogram that was recorded immediately after the stripping experiment (inset, curve c).

The results of stripping experiments argued for the intimate mixing or new compound formation in the film II. We hypothesized that a new compound, for example, a pyrochlore A$_2$B$_2$O$_{7-x}$ (A = Pb, B = Ir),[44] was formed on the electrode surface during electroplating from aged solutions of iridium and lead salts. A pyrochlore is a mixed metal oxide with oxygen vacancies ($x > 0$) and metal centers that can have multiple oxidation states. The pyrochlore hypothesis was consistent with the following observations. The Ir/Pb stoichiometry of pyrochlore (1:1) is the same as that determined for the PbIrOx films (Figure 5, full circles). In the pyrochlore structure, the B and A cations interact through B−O−A linkages,[44] which is consistent with the electroplating of iridium−lead complexes having Ir−O−Pb cores. The high-T pyrochlore powder displayed a pattern of voltammetric peaks that was analogous to that of a PbIrOx film (Figure 6, inset). Finally, the EDX analysis of a PbIrOx film before and after a stripping experiment showed that the atomic % of Pb and Ir remained constant within an experimental error (±15%), which indicated a good stability of the PbIrOx phase.

Synergistic Catalytic Effects at PbIrOx Films Electroplated from Aged Solutions. The oxidation of carbohydrates was used to probe the electrocatalytic properties of PbIrOx films. Initial studies at $E = 0.750$ V showed that the oxidation of carbohydrates took place at Ir(IV) sites of PbIrOx films because no carbohydrate oxidation was observed at PbOx films. For example, the current due to oxidation of glucose increased with the Ir content in PbIrOx films and reached a plateau at the atomic ratio Ir/Pb $\cong$ 1. The activity of such films toward the oxidation of eight other mono- and disaccharides was investigated and compared with the activity of IrOx films. The experiments
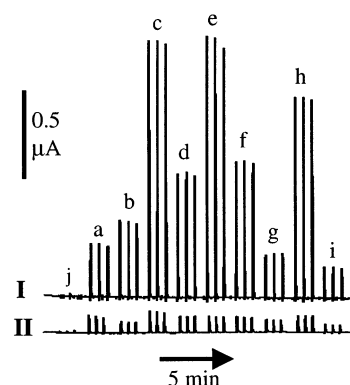
described below were done using two film electrodes, PbIrOx and IrOx, which yielded fingerprint voltammograms c and a, respectively (Figure 4).

Figure 7 shows amperometric traces ($E = 0.750$ V) that were recorded at a PbIrOx (trace I) and IrOx (trace II) film electrode in a flow system during injections of selected carbohydrates. The PbIrOx film generated much larger current peaks due to oxidation of carbohydrates, which could be explained by a larger content of active Ir(IV) sites in the PbIrOx than in the IrOx film (see curves c and a, respectively, in Figure 4). The second important feature was that the PbIrOx film enhanced the oxidation of different carbohydrates to a different level; for example, the currents of mannose (c), fructose (e), and arabinose (h) increased the most. This could not be explained in terms of the film's Ir content because the ratio of redox active Ir sites in the two films (Q_{PbIrOx}/Q_{IrOx}) was constant and the same for all of the carbohydrates investigated. Based on the integration of voltammograms of PbIrOx and IrOx films (Figure 4, curves c and a), the ratio Q_{PbIrOx}/Q_{IrOx} was equal to 4.0 ± 0.1. However, the current ratio $I_{Carb@PbIrOx}/I_{Carb@IrOx}$ was larger than that for most of the carbohydrates studied (Figure 7).

The above observations suggested that Pb sites played a role in the amplification and differentiation of carbohydrate oxidation currents at a PbIrOx film. Considering that Pb(II) ions form weak complexes with carbohydrates (K < 40) in aqueous solutions,[45] one could postulate that similar complexation took place between the film's Pb(II) sites and carbohydrates. This resulted in the Pb(II)-induced retention of carbohydrate molecules at the film/solution interface and, thus, allowed for their more efficient oxidation at the adjacent Ir(IV) sites. The current differentiation resulted from different degrees of carbohydrate retention on the film's surface, which was related to the strength of Pb(II)-carbohydrate surface complexation.

Such an explanation of current amplification and differentiation at a PbIrOx film was tested using data on the ligand-exchange chromatography (LEC) of carbohydrates.[46] In the LEC, the carbohydrates are separated on a resin-based column that contains electrostatically immobilized metal ions (e.g., Pb(II)) using water as the mobile phase. Figure 8 shows a correlation between the carbohydrates' retention times on a LEC

(44) Koo, H.-J.; Whangbo, M.-H.; Kennedy, B. J. *J. Solid State Chem.* **1998**, *136*, 269−273.

(45) Mihalick, J. E.; Griffiths, W. P., III; Muten, J. E.; Olson, T. A.; Hein, J. B. *J. Solution Chem.* **1999**, *28*, 1019−1030.
(46) Stefansson, M.; Westerlund, D. *J. Chromatogr. A* **1996**, *720*, 127−136.
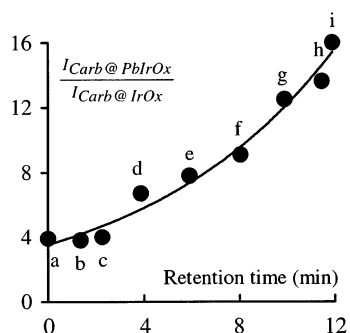
Figure 8. Plot of a ratio of carbohydrate oxidation currents at PbIrOx and IrOx film electrodes (taken from Figure 7) vs carbohydrate retention time[46] on the chromatographic Pb(II) ligand-exchange column. Retention times were normalized by subtracting the retention time of sucrose. Carbohydrates: (a) sucrose, (b) maltose, (c) lactose, (d) glucose, (e) xylose, (f) galactose, (g) arabinose, (h) mannose, (i) fructose.

Pb(II) column[46] and enhancement in the carbohydrate oxidation current at a PbIrOx film, $I_{Carb@PbIrOx}/I_{Carb@IrOx}$ (based on data in Figure 7). A direct proportionality between the current enhancement and chromatographic retention time supported the hypothesis of a synergism involving carbohydrate retention at Pb(II) sites and oxidation at Ir(IV) sites of a PbIrOx film.

Synergistic oxidation mechanisms have been previously considered at catalytic surfaces that contained heavy main group elements. For example, the preadsorption at bismuth sites has been proposed for the oxidation of sulfur compounds at Bi(V)-doped PbO_2 electrodes.[11] The complexation of glucose by the adsorbed oxidized Bi species has been suggested in the mechanism of glucose oxidation at the Bi-modified platinum electrodes.[10] The inhibition of adsorption of poisonous oxidation products by main group elements has been proposed as an explanation for the improved catalytic performance of Bi- and Pb-modified platinum[9] and Pb−Pt alloy electrodes[3] during the oxidation of glucose.

The correlation between the electrochemical and chromatographic data in Figure 8 suggested that (1) the mechanism of carbohydrate oxidation at Ir sites of both the PbIrOx and IrOx films was similar and (2) the mechanism of LEC separation of carbohydrates, in particular monosaccharides d−i, was dominated by a ligand exchange rather than steric exclusion or partitioning on a resin-based Pb(II) column. In addition, such a correlation suggested that Pb−Ir−O pyrochlore could be used as a new stationary phase for the LEC separations of carbohydrates, which is important for further progress in carbohydrate chemistry.

Conclusions

The formation of an ion pair complex between the Pb(II) ion and partially aquated complex $Ir(H_2O)Cl_5^{2-}$ resulted in a remarkable synergistic effect, which allowed for electrosynthesis of a mixed metal oxide PbIrOx having Ir/Pb stoichiometry (1:1) equal to that of the high-temperature Pb−Ir−O pyrochlore. The electrocatalyst PbIrOx enhanced the oxidation of carbohydrates by a synergistic mechanism that involved carbohydrate complexation at Pb(II) sites and oxidation at Ir(IV) sites on the PbIrOx surface.

In a larger perspective, preliminary results indicate that synergistic electroplating of ion pair charge-transfer complexes can be applicable to some other transition/posttransition metal redox systems. The potential generalization of this concept will provide access to new electrocatalysts with enhanced reactivity for a variety of applications, for example, modification of microfluidic devices (lab-on-chip) with catalytic dots of mixed metal oxides for analytical and synthetic purposes. The inadvertent outcome of this work is that solids based on the Pb−Ir−O system may be suitable for the development of new stationary phases for chromatographic separations of carbohydrates.